PCCP

ROYAL SOCIETY OF CHEMISTRY

PAPER

View Article Online
View Journal

Cite this: DOI: 10.1039/d2cp03481f

A combined molecular dynamics simulation and DFT study on mercapto-benzamide inhibitors for the HIV NCp7 protein

Cardia R.,[ab] Cappellini G.,[ac] Valentini M.[b] and Pieroni E.*[b]

Molecular dynamics and quantum simulations are performed to elucidate some aspects of the action mechanism of mercapto-benzamides, a proposed class of antivirals against HIV-1. These molecules act as prodrugs that, after modifications in the biological environment, are able to denature the HIV nucleocapsid protein 7, a metal binder protein, with two zinc finger motifs, vital for RNA maturation and viral replication. Despite their attractive features, these molecules and their biological target are not well understood. Simulations were performed to support a proposed action mechanism, based on the activation of mercapto-benzamides by acetylation, targeting a relatively rare protein hydrolyzed state, followed by *trans*-molecular acetylation from the molecule to the protein and finally the direct interaction of the molecular sulphur atom of mercapto-benzamides with the zinc atom coordinated by the protein. Our simulation results are in agreement with the NMR data about the zinc finger binding protein equilibrium configurations.

Received 29th July 2022,
Accepted 4th October 2022

DOI: 10.1039/d2cp03481f

rsc.li/pccp

Introduction

In recent years, the treatment of acquired immunodeficiency syndrome (AIDS), caused by human immunodeficiency virus 1 (HIV-1), has made great advances, due to the development of highly effective antiretroviral combined therapies.[1,2] Such therapies are partly able to transform the severe pathological condition into a chronic disease state, although with the presence of adverse side effects, often delayed and severe, cost issues (and thus world-wide treatment access difficulties) and above all the drug resistance onset.[3,4]

A class of new viral maturation inhibitors have been proposed[5,6] and have recently been tested *in vitro* and in animal models.[7] These antivirals are based on structural modifications of a benzamide core bound to a thiol derivative group, which presents an active sulfhydryl group. Mercapto-benzamide (MB) compounds can be easily and economically synthesised and are quite well tolerated by animal models. They base their antiviral properties on the ability to denature the HIV-1 nucleo-capside protein 7 (NCp7), a metal binding protein, with two zinc-finger motifs, thus impeding effective viral replication.[5–7]

The NCp7 zinc-knuckle is a structure with three cysteines and one histidine, coordinating a central zinc atom (Fig. 1). This motif is fundamental for the protein's function of binding and stabilising viral RNA. Zinc coordination is pivotal for the correct folding of the protein, which is essential for viral replication and maturation.[5,6] Due to its relevance for virus reproduction, the NCp7 gene is little or not mutated across HIV strands and undergoes relatively marginal mutation even upon host infection, in contrast to what occurs with genes targeted by other drugs.[5,6] Therefore, inhibition of NCp7 is a very attractive

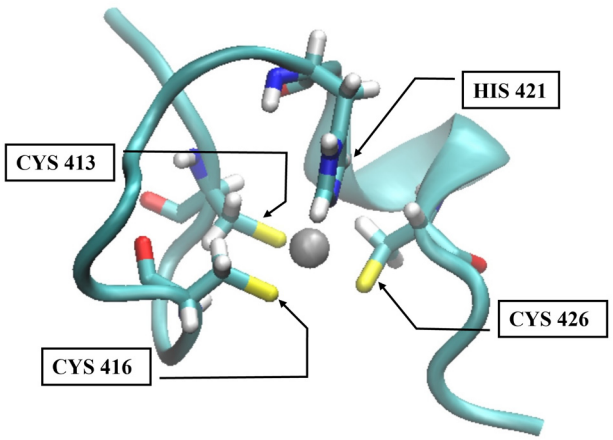

Fig. 1 HIV nucleocapsid protein 7 (NCp7) C-terminal zinc finger motifs (referred in text as model Ω). The four highlighted residues (CYS 413, CYS 416, HIS 421 and CYS 426) are those bonded to the Zn central atom (Zn atom in grey, S in yellow, H in white, N in blue and O in red).

[a] *Dipartimento di Fisica, Università di Cagliari, 09042, Cagliari, Italy*
[b] *CRS4, Modelling, Simulation and Data Analysis Program, 09010, Pula, Italy. E-mail: ep@crs4.it*
[c] *ETSF, European Theoretical Spectroscopy Facility, Italy*

antiretroviral mechanism, able to get rid of viral survival strategies based on frequent mutations and adaptations to therapies, even upon host infection.[8]

The presented facts, in principle, pave the way for the development of a new class of low-cost, effective and well tolerated HIV-1 antivirals targeting NCp7. Unfortunately, NCp7 is a relatively difficult biological target. In particular, zinc-finger motifs exist in the biological environment as an equilibrium of distinct structures, of which the most relevant for the inhibitory effect seems to be the rarer one.[9,10] On the other hand, even MBs are potentially able to coexist in the body in distinct chemical structures. For this reason, MBs are thus able to bind other targets or the same targets in distinct configurations.[11] Therefore, to date, we miss a coherent frame to understand the MB-NCp7 interaction in its entireness.[12–14]

The interaction mechanism recently proposed[10,11] is that, in the body biological environment, the MB247 molecule (Fig. 2A) is acetylated to the form AcMB247, where the thiol SH group is replaced by the acetyl group SOCH3 (Fig. 2B). On the other hand, the NCp7 (C-terminal) finger motif fully coordinating a zinc atom is in equilibrium with its other two hydrolyzed structures. Among these three equilibrium structures, the one relevant for our purposes is the structure C represented in Fig. 3. This structure is characterised by hydrolyzed cysteine, namely CYS413, which is thus partly freed by the central zinc

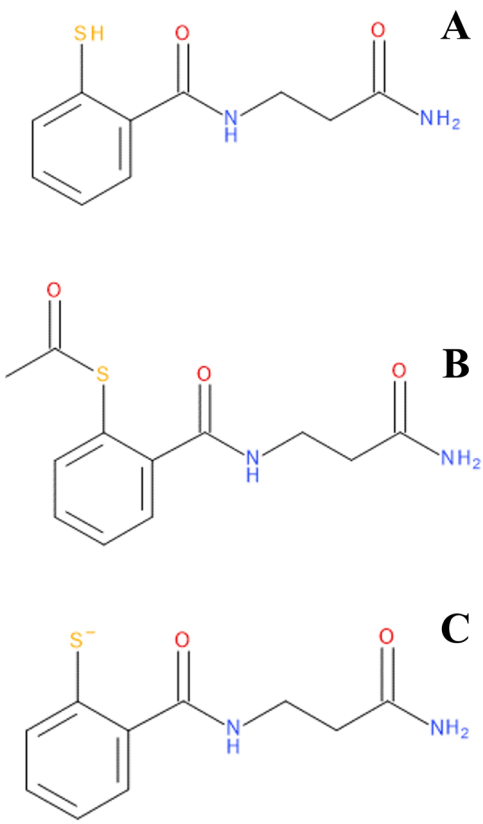

Fig. 2 MB247 mercapto-benzamide inhibitor in the (A) standard form, (B) acetylated form AcMB247 and (C) corresponding ionised form after zinc finger motif transacetylation.[5–7]

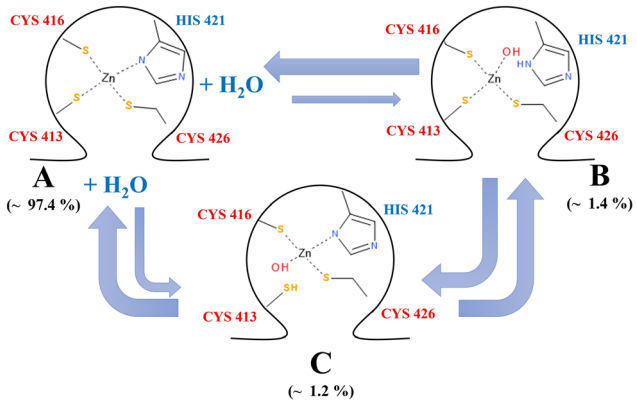

Fig. 3 The three equilibrium configurations of the NCp7 zinc-knuckle motif. The crystallographic structure (PDB id 2L44) is represented by (A). The two hydrolyzed rare equilibrium configurations are represented by (B and C). The proposed MB247 action mechanism targets the NCp7 protein in its form (C). This model is proposed in the published literature on the basis of purely experimental data.[10,11]

atom coordination. Therefore, when the AcMB247 molecule interacts with the zinc finger motif in the C-form, the acetyl group is transferred from AcMB247 to NCp7 CYS413 (Fig. 4). Moreover, the MB247 sulphur atom, now free and negatively charged (Fig. 2C), interacts directly with the motif coordinating zinc, thus interfering with the zinc coordination exerted by the remaining two cysteines and one histidine. The presented process eventually leads to protein misfolding or even unfolding. The full mechanism path is presented in Fig. 5. Accordingly, to the model proposed in the literature,[10,11] the next step (not simulated in the present work) is the intramolecular transfer of the acetyl group from CYS413 to the region close to LYS415, thus allowing the sulphur atom on CYS413 to create disulfide bonds and thus helping in the zinc ejection. Finally, we briefly present three more details of the MB-NCp7 interaction that are to date poorly understood and deserve to be

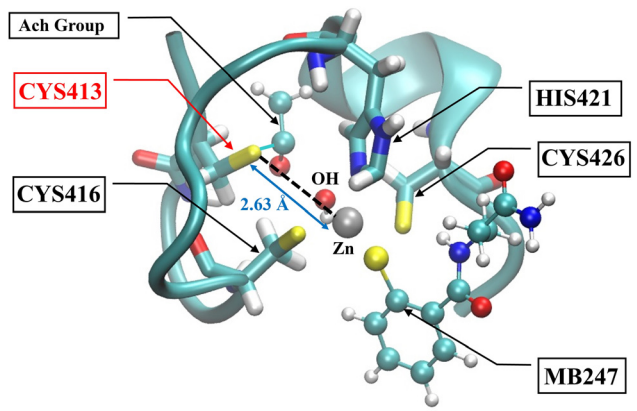

Fig. 4 Model *AcHΩ*, used as the initial configuration for the DFT simulation, in balls and sticks representation. The acetyl group is linked to CYS413, due to transacetylation from AcMB247. The OH group is bonded to Zn (grey) as an effect of hydrolysis, with a position and orientation derived from the output of the MD in the explicit water simulation (C atoms in green, S in yellow, H in white, N in blue and O in red).

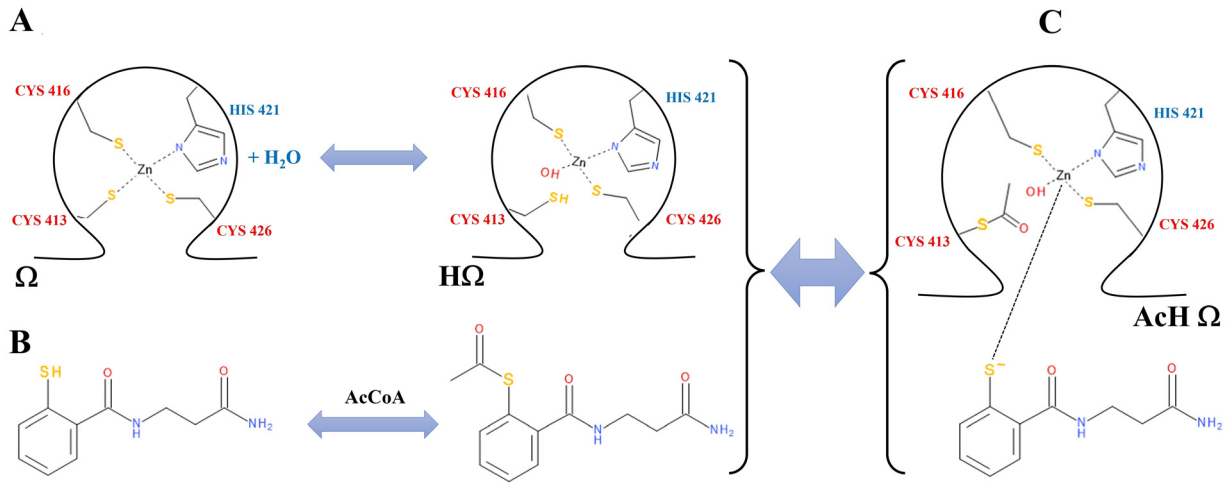

Fig. 5 Proposed[10,11] action mechanism of MB247 for NCp7 inhibition. (A) Motif form Ω (Fig. 3A) is in equilibrium with the hydrolyzed form *HΩ* (Fig. 3C). (B) MB247 in equilibrium in the body with its acetylated form, thanks to the mediation of acetyl-coenzyme (A). (C) Acetylated MB247 reacts with the hydrolyzed form *HΩ* by first transferring the acetyl group to CYS413. The resulting products, namely the ionised active MB247 and the *AcHΩ* motif (both reported in the picture), react together by the S–Zn direct interaction.

elucidated.[7,8] First, the MB inhibitory action against NCp7 is highly modulated by the structural details of the specific MB molecule, with IC50 values ranging from 1 μM to 100 μM, strongly depending on very subtle changes to the aromatic ring and chain composition. Second, some MB structures are active *in vitro* while they lose their effectiveness *in vivo*. The last fact is that the NCp7 protein is made up of two zinc finger motifs, but only the C-terminal one is involved in the inhibitory action by MBs. In this paper, we briefly discuss only the first point, the subject of our previous quantum simulation work.[15]

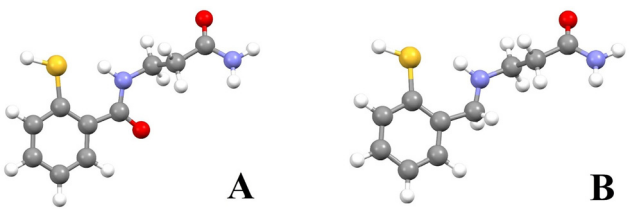

Fig. 6 (A) Effective MB247 inhibitor (Fig. 2A) and (B) a slightly modified version, with oxygen replaced by two hydrogens. C atoms are colored in grey, S in yellow, O in red, N in violet and H in white.

Molecular modelling

We adopted a combination of classical and quantum *ab initio* techniques in order to study the inhibitory action of the MB molecules on the HIV-1 NCp7 protein, in accordance with the last published findings and hypotheses on the MB action mechanism.[10,11]

At first, the rationale behind the modelling protocol is presented, and subsequently, the details are discussed. From the PDB databank, we obtained a 3D structure of the NCp7 zinc-knuckle region with a coordinated central zinc atom, namely model #1 of the PDB ID 2L44 NMR bundle.[16,†] This is used as the reference structure to build a reliable molecular homology model[17] Ω for the C-terminal zinc finger motif (chain 1 in the 2L44 structure, Fig. 1). In our previous work, the Ω model was subjected to two quantistic DFT simulations, in a vacuum and in implicit water environments. In both cases, the zinc finger motif remained stable and misfolding was not observed.[18,19] We also performed the quantum simulation of the interaction between the Ω motif and different MB molecules. In this way, we showed that a specific MB molecule, namely MB247 (Fig. 2B and 6A), has the potential to denature the zinc finger motif (Fig. 1), while a slightly modified version of it (Fig. 6B) does not.[7,8,15] Back to the present work, the second step of our study was to perform the molecular dynamics (MD) simulation[20] of the model Ω in water and to identify the closest water molecule to zinc during system evolution. Precisely, this water molecule was used to hydrate the finger motif. By hydration we mean the binding of an oxydrile group to the coordinated zinc and an hydrogen atom to the sulphur group of a specific cysteine side chain (Fig. 3). In this way, we obtained the target structure that is truly active for the inhibitory effect, the hydrolyzed motif *HΩ* (Fig. 4). As extra bonuses we obtained (i) the model Ω refinement and energy minimisation in explicit water and eventually (ii) the sampling of the three Ω equilibrium configurations (Fig. 3). It should be noted that MB247 was not subjected to the MD simulation. In this way, we were able to build an MD-based accurate model of the Zn finger hydrolyzed motif *HΩ*. In turn, this motif will be acetylated positioning manually the acetyl group to simulate the initial interaction with the deacetylated active MB247 molecule and to prepare the initial state for the quantum simulation. More precisely, an acetyl group was migrated from acetylated MB247 to the CYS413 sulphur atom, thus obtaining the model *AcHΩ* (Fig. 4). The final model *AcHΩ* and the active ionised MB247 molecule (Fig. 2C) were thus

† PDB structure at **https://www.rcsb.org/structure/2L44**.

subjected to the DFT simulation in the implicit water environment to eventually observe motif denaturation.

Therefore, we combined the best of two worlds. We adopted the MD simulation in water to identify the most accurate model for the hydrated protein, being impossible for computational reasons to insert a large number of explicit water molecules in the DFT simulation. In this way, as added values, we optimised the structure in water and confirmed the proposed protein equilibrium configurations. On the other hand, MD requires too long simulation times to model charged systems and to highlight the formation of new bonds, while DFT can perform both these tasks efficiently and fairly accurate.

Materials and methods: molecular dynamics

MD simulations have been performed using NAMD.[21] We selected model #1 from the PDB NMR structure 2L44[16,†] for the C-terminal zinc knuckle of the HIV-1 NCp7 protein.‡ The structure consists of 19 amino acids, representing the zinc knuckle motif,§ corresponding to NCp7 protein amino acids 411–429. Starting from this model we built a cubic simulation box of dimensions [82.55 Å, 78.55 Å, 74.65 Å], obtained by solvating the protein with 16088 water molecules described by TIP3P potential.[22]

The size of the simulation box and of the water layer around the protein is chosen large enough to prevent edge artefacts due to periodic boundary conditions. The system topology was constructed using VMD[23] autopsf routines¶ using the CHARMM36 force field.[24] To preserve the motif structural peculiarities, given the short amino acid sequence, we have minimised the energy and performed MD simulations keeping the backbone atoms fixed. The unrestrained MD simulation of this short 19 amino acid chain is too unstable to be significant, while the fixed backbone approach allows the rearrangements of the side chains to be observed, which are the keys through which the MB247–motif interaction mechanism acts. We selected the lowest energy model (namely #1) from the PDB NMR bundle, but we also checked that the 20 NMR models display a very little deviation of the backbone (RMSD = 0.16A), thus further confirming that the restrained MD simulation is appropriate. An initial MD equilibration of the system has been achieved by 1000 ps simulation steps. This short run served to minimise the energy – through the conjugate gradient method – and to relax any atomic contact eventually present in the initial configuration. A subsequent MD run has been performed in the NPT ensemble, with an initial temperature of 310 K, maintained using a Langevin thermostat with a damping coefficient of 1 ps^{-1} and the pressure was kept constant by the Nosé–Hoover Langevin method at 1.03 bar, with a period of 100 fs and a decay time of 50 ps. Long-range Coulomb interactions are treated by Particle Ewald Mesh with a tolerance of 10^{-6}, a Ewald coefficient of 0.257 and a grid size of [84 Å, 80 Å, 80 Å]. The molecular dynamics was carried out up to an overall duration of 136 ns, with an integration time step of 2 fs and constraining the bonds involving hydrogen. The system configurations were saved every 5000 time integration steps in order to obtain the trajectories for the subsequent analysis. This protocol is fairly standard and adopted by many authors for the protein simulation.[25,26]

Materials and methods: DFT

We have performed all the calculations within the density functional theory (DFT)[18,19] framework, as implemented in the GAUSSIAN16[27] package. In detail, we performed the geometrical optimization of the structure using the Berny structural relaxation algorithm,[28] with the following convergence criteria: maximum force = 1.5×10^{-5} Ha/Bohr, RMS force = 1.0×10^{-5}, maximum displacement = 3.0×10^{-5} Å and RMS displacement = 4.0×10^{-5} Å‖.

Geometry optimizations have been obtained using the Becke three-parameter Lee–Yang–Parr (B3LYP) hybrid exchange correlation functional,[29,30] which has proved to have a stable behaviour, with few well-documented limitations.[31] Our investigation involves only the study of the structural behaviour of the system and not an analysis of the excited states; therefore, it was not necessary to use the diffuse function basis sets. The extra bonus is a smaller computational effort to reach convergence. In this framework, we can thus approximate the wave functions using the Pople 6-31G* basis-set,[32] a valence double-ζ set augmented with *d* polarisation functions. The structural optimization of the system was performed without imposing symmetry constraints. The procedure described has been successfully tested for many different atomic systems, both organic and inorganic, with different sizes and degrees of complexity.[33–39] Before the DFT simulation, the system is pre-optimised using the Avogadro internal optimization tool and the General AMBER Force Field, with default parameters.[40]

We observe that, being mainly interested in the evolution of the protein structure, we can perform simulations with a higher total number of atoms than that normally used in the standard DFT structural optimization. The simulations were performed using a reliable implicit solvent model, namely the density corrected polarizable continuum model,[41,42] in order to take into account at least the first order effects of the water environment in cells. The DFT calculations also allowed the exact ground state to be obtained for binding molecules, the target protein and their complexes.

Results and discussion

The main result can be summarised in two figures: Fig. 4 shows the initial DFT simulation configuration, with the central zinc atom coordinated by the NCp7 motif, while Fig. 7 shows the denatured NCp7 protein and the uncoordinated zinc, due to the effect of the MB247 inhibitor. As anticipated, in our previous work, we showed that this is not an artefact, being the Ω model alone stable during quantum simulations.[18,19] Table 1 reports

‡ HIV-1 NCp7 protein, with Uniprot id Q74084.

§ The zinc finger motif is CYS413-X2-CYS416-X4-HIS421-X4-CYS426.

¶ https://www.ks.uiuc.edu/Research/vmd/plugins/autopsf/.

‖ https://gaussian.com/basissets/.

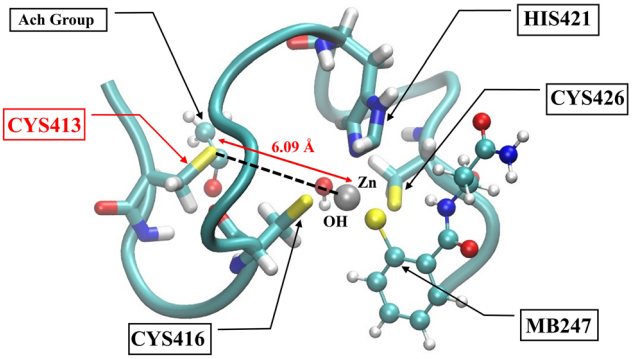

Fig. 7 Final configuration of the DFT simulation. The Zn atom is dislocated (see table Table 1) and the NCp7 protein is misfolded. Colours are shown as in Fig. 4. The dashed lines report the distance in Å.

Table 1 Distances between the zinc atom and the NCp7 residues involved in the zinc coordination (S for CYS or Nε2 for HIS). The first column reports the distances obtained from the crystallographic NMR structure 2L44 (see footnote †).[16] The second (third) column reports the distances at the beginning (end) of the quantum simulation

Distances Zn–CYS/HIS	NCp7 (crys) [Å]	*AcH*Ω-MB247 (t = 0) [Å]	*AcH*Ω-MB247 ($t = t_{fin}$) [Å]
Zn–CYS413	2.30	2.63	6.09
Zn–CYS416	2.27	2.33	2.38
Zn–HIS421	2.05	1.95	2.00
Zn–CYS426	2.37	2.25	2.28

the distances among the coordinating amino acids and the zinc atom for the crystallographic structure and the quantum simulation initial (Fig. 4) and final systems (Fig. 7). In Table 1, the high value obtained for the CYS413–Zn distance at the simulation end is highlighted. The energy trend observed along the DFT optimization ensures that the process is convergent (Fig. 8). The distance between the Zn atom and the NCp7 CYS413 S atom, involved in zinc coordination, is slightly different in the crystallographic data and in the initial model for the DFT simulation (Table 1, first and second columns). This difference is primarily due to the effect of MD in explicit water and secondarily to the preparation of the hydrated and acetylated initial system for the DFT run. In Table 1, it is shown that, after the interaction with MB247, the zinc atom is definitely not anymore coordinated with CYS413. Thus, now the zinc atom is able to interact directly with the MB247 S atom, finally leading to protein misfolding, as reported in Fig. 7. Therefore, provided one carefully prepares the hydrolyzed system, in particular with a MD in explicit water, the DFT simulation of the hydrated motif in implicit water is thus able to show that NCp7 misfolds and ejects the zinc atom under the action of MB247.

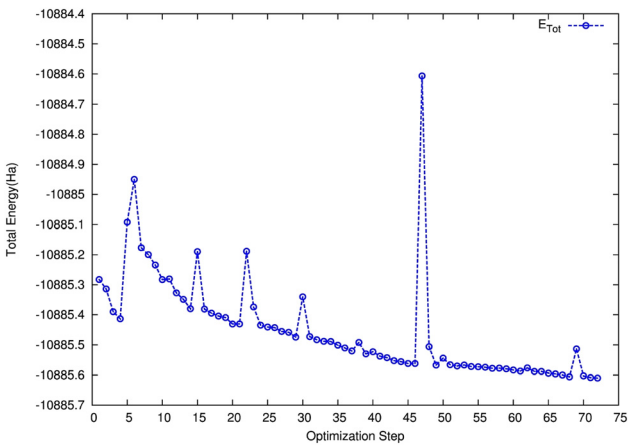

Fig. 8 Total energy of the NCp7-MB247 system during the DFT simulation. The energy values synthesise the system structural evolution that can be interpreted as a protein unfolding process. The relevant aspects are the trend and the convergence of the optimisation process, while the peaks are just artefacts due to eventual temporary steric hindrance or orbital overlaps.

Back to intermediate results, to obtain some clues about the presence of distinct hydrolyzed configurations (Fig. 3), we studied the water molecule dynamics around the protein. Therefore, from the equilibrated part of the MD simulation of model Ω in explicit water (Fig. 1), we extracted the histograms for the distances between the Zn atom and, respectively, the CYS413 sulphur atom (CYS413.S, Fig. 9), the closest water hydrogen (Fig. 10) and the closest water oxygen (Fig. 11). Moreover, we plotted the histogram of the distance between CYS413.S and the closest water H atom (Fig. 12). Similarly, we evaluated the histogram of the distance of the HIS421 Nε2 atom (HIS421.NE2, Fig. 13) from the closest water H atom (Fig. 13). All histograms are evaluated in a 5 Å radius ball from the Zn, S or N atom. All these spheres, at the equilibrium, contain on average two water molecules.

The histogram of the distance Zn-CYS413.S (Fig. 9) represents the harmonic coordination of the Zn atom by CYS413, with an average distance of 2.9 Å. The two histograms Zn–H and Zn–O (Fig. 10 and 11) clearly show the dynamic presence of a close water molecule with an O atom at an average distance of 2 Å from Zn, with other water molecule oxygens quite far away (distance greater than 4 Å). In detail, the MD simulation reduces the Zn–O distance, with the last frames sampling the

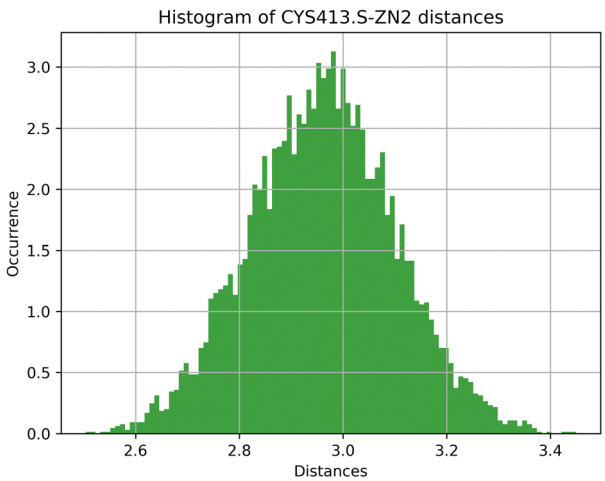

Fig. 9 Histogram of the distance CYS413.S–Zn during MD simulations.

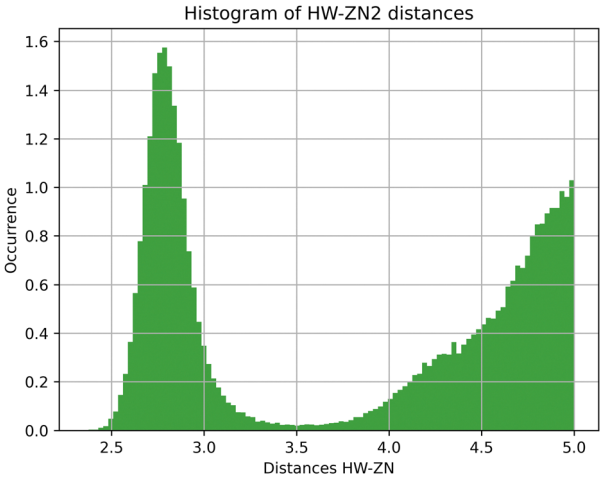

Fig. 10 Histogram of the distance (closest water H)–Zn during MD simulations.

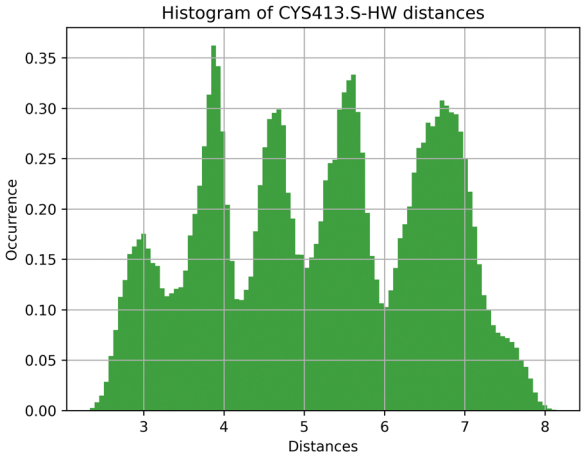

Fig. 12 Histogram of the distance (closest water H)–CYS413.S during MD simulations.

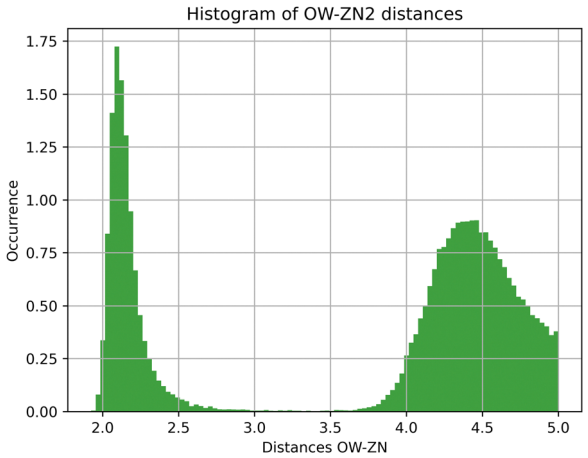

Fig. 11 Histogram of the distance (closest water O)–Zn during MD simulations.

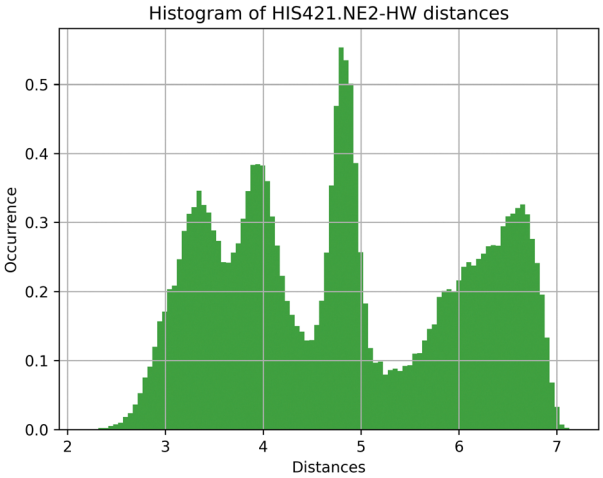

Fig. 13 Histogram of the distance (closest water H)–HIS421.NE2 during MD simulations.

lowest part of the distance distribution (Fig. 11). In particular, the minimal Zn–O distance MD frame, used as an input for the subsequent DFT simulation, displays a Zn–O distance of 1.9 Å. Moreover, this distance changes very little during the quantum simulation, with a final value of 1.8 Å. This is in very good agreement with the typical Zn–O first coordination distance for many species of hydrated zinc, spanning the range 1.8–2.1 Å.[43] Precisely, the position and orientation of the closest water molecule during the simulation was used to hydrate the Zn atom for the subsequent DFT simulation. Furthermore, a hydrogen atom is also sampled at a minimal distance of 2.4 Å from CYS413.S (Fig. 12).

From the histograms in Fig. 10–12, it is evident that the hydrolyzed motif configuration, with OH very close to Zn and H as close as possible to CYS413.S, as allowed by MD force fields, is less frequent than others with farer H atoms and should be the representative of the rare equilibrium configuration C in Fig. 3.

Therefore, we can conclude that the MD of the model Ω in water seems to be able to sample the for-our-purposes relevant hydrolyzed Ω structure (Fig. 3C), coherently with the published experimental data.[10,11] We also observe that using the MD simulation we were able to sample the structure B in Fig. 3, with HIS421.NE2 as close as possible (approximative range of 2.5–3.5 Å from Fig. 13) to an H atom from the closest water molecule.

Fig. 14 reports the highest occupied molecular orbital (HOMO) for the full system, composed by the MB247 molecule and the acetylated and hydrated NCp7. In Fig. 15, a detailed zoom of the molecular orbitals (MOs) is reported and located around the CYS416 and CYS421 residues, Zn atom, OH group linked to Zn, MB247 S atom and ring. From Fig. 14 and the enhanced view reported in Fig. 15, as expected, it is evident that the entire region around the Zn atom represents a very reactive area. The MOs around the MB247 ring and the S atom are a clear signal that this part of the MB247 molecule is

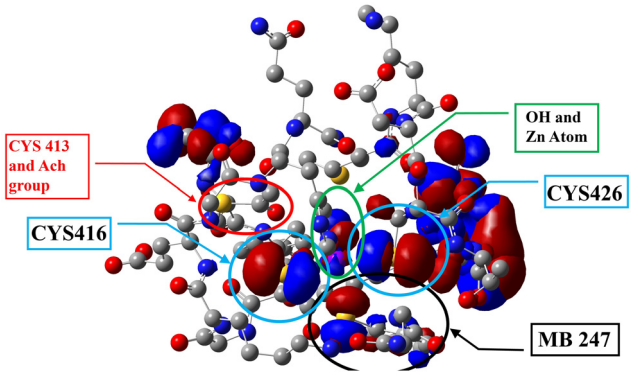

Fig. 14 Isosurface representation of the HOMOs for the full system composed of the acetylated and hydrated zinc finger motif and MB247. The wave function sign is represented by the colour, negative in red and positive in blue.

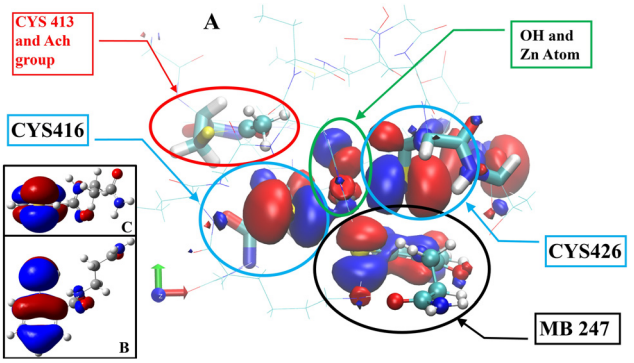

Fig. 15 Zoom of the MOs of Fig. 14 on the area around the Zn atom (A). The two left frames are reported; for comparison, the HOMO of the isolated MB247 molecule (B) in the top view and (C) in the side view, with respect to the molecule plane.

participating in a chemical reaction with NCp7. Comparing the MOs of the isolated molecule MB247 (Fig. 15B and C) with those of the bound molecule (Fig. 15A), it is evident that the MOs around MB247 remain almost unchanged as regards the shape and distribution of the charge. This fact indicates the maintenance of the activity and reactivity of the MB247 compound, even after the transacetylation reaction and binding with Zn.

Conclusions

The action of MB molecules on the HIV zinc-finger protein NCp7 has been analysed with the use of a combined MD and quantum parameter-free scheme, in order to highlight drug action mechanisms and which specific MB and which protein configuration are involved in the MB antiviral effect. The NCp7 zinc-finger protein has been modelled by MD in explicit water to prepare the hydrolyzed model and sample its distinct hydrolyzed equilibrium configurations. This resulted in identifying the closest water molecule to zinc. This water molecule will be explicitly embedded in the DFT simulation. The DFT simulation involved the de-acetylated charged active form of MB247 and the acetylated and hydrolyzed NCp7 structure identified as the antiviral target. To deal with charged molecules and build up reactive chemical reactions, the quantum simulation was performed. The present work integrates and extends our published preliminary study, where we observed that the zinc finger motif not interacting with the MB247 molecule was stable.

The results obtained here showed that acetylated MB247 is able to induce misfolding in the target hydrolyzed NCp7 zinc-finger motif. This is due to the subsequent combined action of (i) weak zinc coordination by CYS413 in the rare hydrolyzed structure, (ii) further zinc coordination weakening by transacetylation of CYS413 from acetylated MB247, (iii) zinc coordination sharp rerouting from CYS413 to the charged sulphur in MB247. All these steps resulted in zinc ejection, eventually helped by the final intra-protein acetyl group transfer from CYS413 to LYS415.

Overall, the results presented unveil specific MB HIV-1 antiviral properties, explain some experimental results and confirm the proposed pro-drug action scheme. The presented approach can be extended to study the NCp7 rare equilibrium hidden states that could be targeted by antivirals, the role of MB structural changes and the CYS–LYS intramolecular acetylation, thus in general boosting the rational design of MBs with desired HIV-1 antiviral properties.

Conflicts of interest

There are no conflicts to declare.

Acknowledgements

The authors are deeply grateful to Amit Kumar for his careful reading and correction of the English text. The authors acknowledge the HPC group at CRS4 for the use of CRS4 computational facilities and ISCRA-CINECA facility within the ISCRA-C 2021 project HP10CDZJIB. G. C. acknowledges collaboration with ''Progetti biennali d'Ateneo UniCa finanziati dalla Fondazione di Sardegna annualità 2020: Molecular simulations and machine learning in bio- and medical physics'', and partial financial support from the IDEA-AISBL-Bruxelles. The authors warmly thank Daniel Appella for bringing this interesting research topic to their attention.

Notes and references

1 P. Jain, *et al.*, *Crit. Rev. Anal. Chem.*, 2022, **26**, 1–15.
2 Y. Zhang, *et al.*, *J. Int. AIDS Soc.*, 2022, **25**(4), e25902.
3 S. Y. Rhee, *et al.*, *Lancet Microbe*, 2022, **3**(5), e392–e398.
4 M. A. Boyd, *et al.*, *Curr. Opin. Immunol.*, 2022, **76**, 102186.
5 G. R. Rice, *et al.*, *Science*, 1995, **270**, 1194.
6 J. M. Domagala, *et al.*, *Bioorg. Med. Chem.*, 1997, **5**, 569.
7 T. L. Hartman, *et al.*, *Antiviral Res.*, 2016, **134**, 216–225.

8 M. Saha, *et al.*, *Chem. Med. Chem.*, 2017, **12**, 714–721.
9 L. Deshmukh, *et al.*, *Angew. Chem. Int. Ed.*, 2018, **57**(10), 2687–2691.
10 H. Nikolayevskiy, *et al.*, *Chemistry*, 2018, **24**(38), 9485–9489.
11 H. Nikolayevskiy, *et al.*, *Eur. J. Med. Chem.*, 2019, **178**, 818–837.
12 L. Sancineto, *et al.*, *Drug Discovery Today*, 2018, **23**(2), 260–271.
13 N. Iraci, *et al.*, *Drug Discovery Today*, 2018, **23**(3), 687–695.
14 V. Shvadchak, *et al.*, *Biochemistry*, 2018, **57**(30), 4562–4573.
15 (*a*) G. Cappellini *et al.*, Proceedings Nanoinnovation-21 Congress, Rome September 2021, IOP (in press); (*b*) R. Cardia, *et al.*, *Nuovo Cimento C – Colloquia and Communications in Physics*, 2022, **45**, 192.
16 S. Quintal, *et al.*, *Biochemistry*, 2012, **51**, 1752–1761.
17 C. Chothia and A. M. Lesk, *EMBO J.*, 1986, **5**(4), 823–826.
18 W. Kohn, *et al.*, *Rev. Mod. Phys.*, 1999, **71**, 1256.
19 R. O. Jones, *et al.*, *Rev. Mod. Phys.*, 1989, **61**, 689–746.
20 A. Rahman, *et al.*, *Phys. Review.*, 1964, **136**(2A), A405–A411.
21 J. C. Phillips, *et al.*, *J. Chem. Phys.*, 2020, **153**, 044130.
22 A. D. MacKerell, *et al.*, *J. Phys. Chem.*, 1998, **102**, 3586.
23 W. Humphrey, *et al.*, *J. Molec. Graphics*, 1996, **v. 14**, 33–38.
24 J. Huang, *et al.*, *Nat. Methods*, 2016, **14**, 71–73.
25 A. Kumar, *et al.*, *Mol. BioSyst.*, 2014, **10**(8), 2043–2054.
26 A. Kumar, *et al.*, *Sci. Rep.*, 2018, **8**(1), 4424.
27 M. J. Frish *et al.*, *Gaussian16 Rev. C.01*, 2016.
28 H. B. Schlegel, *et al.*, *J. Comp. Chem.*, 1982, **3**, 214.
29 A. D. Becke, *et al.*, *J. Chem. Phys.*, 1993, **98**, 5648–5652.
30 C. Lee, *et al.*, *Phys. Rev. B: Condens. Matter Mater. Phys.*, 1988, **37**, 785–789.
31 S. Grimme, *et al.*, *Chem. Phys. Chem.*, 2003, **4**, 292–295.
32 R. Ditchfield, *et al.*, *J. Chem. Phys.*, 1971, **54**(2), 724–728.
33 G. Malloci, *et al.*, *Phys. Rev. B: Condens. Matter Mater. Phys.*, 2004, **70**, 1–6.
34 R. Cardia, *et al.*, *J. Phys. Chem. A*, 2014, **118**, 5170–5177.
35 N. Dardenne, *et al.*, *J. Phys. Chem. C*, 2017, **121**(44), 24480.
36 P. Mocci, *et al.*, *Phys. Chem. Chem. Phys.*, 2019, **21**, 16302.
37 G. Cappellini, *et al.*, *ACS Omega*, 2020, **5**(22), 13268–13277.
38 A. Kumar, *et al.*, *Cellulose*, 2017, **25**(4), 2191.
39 L. Stagi, *et al.*, *Spectrochimica Acta A*, 2017, **183**, 348–355.
40 M. D. Hanwell, *et al.*, *J. Cheminform.*, 2012, **4**, 17.
41 J. Tomasi, *et al.*, *Chem. Rev.*, 2005, **105**(8), 2999.
42 A. V. Marenich, *et al.*, *J. Phys. Chem. B*, 2009, **113**, 6378.
43 M. Zhu, *et al.*, *J. Phys. Chem. A*, 2005, **109**, 7648–7652.

